17 Nanolithography in the Evanescent Near Field

M. M. Alkaisi and R. J. Blaikie

MacDiarmid Institute of Advanced Materials and Nanotechnology, University of Canterbury, New Zealand

17.1 Introduction

The ability of nanotechnology to manipulate systems down to the scale of individual atoms and molecules offers exciting potential for novel devices and materials. It is expected that significant progress in science and technology will be achieved. As a result, considerable interest in developing new nanofabrication techniques for manufacturing nanoscale structures has emerged worldwide. Techniques such as nano-imprint lithography, microcontact printing, immersion lithography and electron projection lithography offer alternatives to conventional electron beam nanolithography or recently developed EUV lithography. Many of these alternatives offer advantages of low cost and high throughput for mass production of nanostructured materials and devices.

The resolution of conventional projection optical lithography is limited by diffraction, making it extremely challenging to fabricate sub-100 nm structures even using deep UV light sources and advanced wavefront engineering. However, by working in the optical near field the conventional diffraction limit can be overcome and nanoscale patterning can be achieved. Whilst this idea is not new it is only relatively recently that detailed studies have been performed. The first demonstrations of sub-wavelength resolution near field nanolithography used serial scanning techniques which is not suitable for high throughput lithography process, however in this Chapter we will be presenting the implications of using evanescently decaying components in the near field of a photomask as a parallel lithography tool for the fabrication of nanoscale structures.

Both experimental and simulation results for evanescent near field optical lithography (ENFOL) will be discussed. The ENFOL technique allows for sub-diffraction-limited resolution to be achieved with optical lithography by keeping a shadow mask in intimate contact with an ultra-thin photoresist layer during exposure – this ensures that the photoresist receives exposure from the evanescently decaying diffracted orders in the near field of the mask. Features as small as 70 nm on a 140 nm period have been patterned using broadband UV illumination

(365-600 nm), and subsequently transferred these patterns into silicon using reactive ion etching (RIE) (Blaikie et al. 1999; Alkaisi 2001). This resolution is below the conventional diffraction limit for projection optical lithography and illustrates the promise for extending optical lithography into the sub-100 nm realm. Simulation studies have shown that resolution down to 20 nm should be possible with this technique (McNab and Blaikie 2000), an enticing prospect for the nanolithographer.

The rest of this chapter will be structured as follows. We will first briefly review the historical development of near field contact lithography, outline the principles of the ENFOL technique and give details of the techniques required for the fabrication of conformable near field masks. Experimental results demonstrating the resolution that can be achieved with ENFOL exposure into ultra-thin photoresists are presented. Details of the subtractive and additive pattern transfer processes that have been developed are presented. Simulation results are also shown. This indicates that the resolution limits for ENFOL have yet to be reached experimentally. Finally, advanced near field lithography techniques such as evanescent interferometeric lithography, planar lens and surface plasmon lithography will be discussed.

17.2 Historical Development

An essential requirement for near field photolithography techniques such as ENFOL is to maintain a conformable photomask in intimate contact with the photoresist during exposure. The first work using conformable photolithography masks was reported by Smith in 1969 for fabricating surface acoustic wave (SAW) devices. Mechanical pressure was used to maintain contact and interdigital electrodes with 2.5 μm periods were replicated. In later work Smith demonstrated 400 nm linewidths on an 800 nm pitch using the same technique but this time using vacuum pressure to attain intimate contact between the mask and substrate. A distinct advantage of this system is the insensitivity of the linewidth to exposure time when operating in true intimate contact. In that paper Smith hints at the prospect of achieving higher resolutions – "Although no effort has been made to explore the ultimate limitation of the conformable mask photolithography, our observations lead us to speculate that narrower linewidths than reported here are probably possible, but may require the exercise of finer control over photoresist thickness and exposure parameters". These words turned out to be quite accurate, although were not realised until nearly a decade later, when White et al. demonstrated patterning of 150 nm features with a 157 nm laser source (White et al. 1984). A further important advantage of the conformable mask that is cited is the absence of damage or wear through repeated use (Smith et al. 2000), an improvement on the conventional photomasks which suffer degradation with use.

Goodberlet has used a modification of the conventional conformable mask, where the absorber is embedded into the mask substrate. His embedded amplitude mask (EAM) consists of a substrate material made from fused silica, with

embedded Cr absorber patterns. There are a number of advantages of the having the absorber embedded: a flat mask would be expected to reduce local deformations around the absorber areas, the narrow regions between the absorber also improve waveguiding with their higher refractive index, and the planarity of the mask may protect the absorber and minimise particle contamination. The EAM mask has been used to reproduce 100 nm line and space structures, using a source with a wavelength of 220 nm. Pattern placement errors have been evaluated by Goodberlet by measuring the in-plane distortions of a double exposure with the mask misaligned slightly between the first and second exposure. An average displacement of 58 nm was observed over an area of 2 cm^2. Attempts at multilevel alignment are also in progress. More recently Goodberlet (2002) has demonstrated patterning features down to 45 nm using this technique.

In another technique, light-coupling masks (LCM) for conformable contact photolithography have been developed by a group at IBM's Research Laboratory in Zurich (Schmid et al. 1998). The masks are made of an elastomeric material, similar to that developed for microcontact printing (Rogers et al. 1997), which allows for conformal contact. The mask consists of a surface relief pattern and relies on this pattern to induce local optical modes; this waveguiding action amplifies the intensity in the protruding mask regions, which results in contrast in the underlying resist (Paulus et al. 2001). Another contrast mechanism occurs when the wavelength is much smaller that the features on the mask; if the depth of the surface relief results in a phase change close to π the destructive interference that results at the mask edge results in a strongly unexposed region. The same effect is observed in near field phase shifting masks (PSMs). Results for LCM exposure demonstrate that 240 nm period is possible with a low surface relief pattern (70 nm deep) using 248 nm wavelength exposure. In this case the low surface relief and small size of the patterns means that the second exposure mechanism is not significant.

Fig. 17.1 illustrates the four possible mask configurations for near field lithography. A simulation study comparing the performance of these different techniques has been performed (Paulus etal.2000); whilst the contrast, depth of focus and minimum feature size are slightly improved for the embedded absorber and recessed absorber compared to the protruding absorber, the simplicity of mask fabrication makes the latter technique the best choice in many cases.

An alternative to using a conformable mask with a rigid substrate is to use a rigid mask with a conformable substrate. Ono et al. have replicated 500 nm period structures with such an arrangement. They formed substrates from 1μm silicon diaphragms and performed a contact exposure with standard chrome on glass mask using vacuum pressure and a mercury arc lamp source. However, the use of conformable substrates limits the range of devices that can be fabricated. Near field schemes using conformable masks are much more prominent, and other experimental and simulation studies have appeared in the literature where resolution beyond the diffraction limits have been demonstrated (Haefliger and Stemmer 2004; Luo and Ishihara 2004).

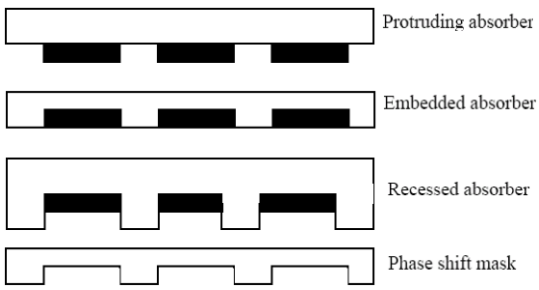

Fig. 17.1. Illustration of the four possible configurations of near field masks, where dark features represent the absorber: (a) is the protruding absorber (b) embedded absorber (Goodberlet 2000), (c) recessed absorber (Schmid et al. 1998; Paulus et al. 2001), and (d) chromeless phase shift mask (Levenson 1993; Alkaisi et al. 1998)

17.3 Principles of ENFOL

The principle of the ENFOL technique is illustrated in Fig. 17.2 A conformable membrane mask is held in intimate contact with a photoresist-coated substrate, such that the mask-substrate gap g (including the photoresist thickness) is much less than the wavelength of the exposing light source. Under these conditions the optical field in the thin resist contains high spatial frequency evanescent components together with propagating diffracted components. The presence of these high frequency components makes resolution beyond the diffraction limit of projection lithography possible.

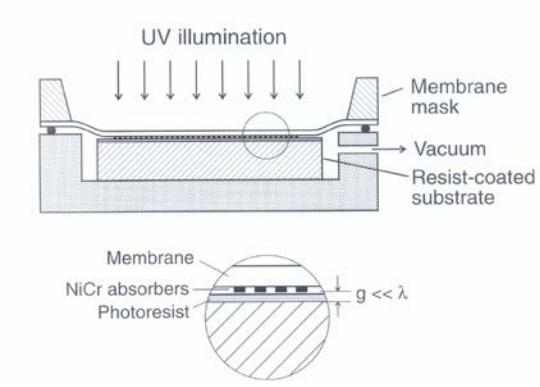

Fig. 17.2. Schematic diagram illustrating the evanescent near field optical lithography (ENFOL) process. Photolithography is performed through a conformable mask held in intimate contact with a resist layer that is much thinner than the illuminating wavelength

As can be seen from Fig. 17.2, the two main requirements for ENFOL are intimate mask-substrate contact over a large area and ultra-thin (sub-100 nm) resists. Using a conformable mask held in contact with the resist by external pressure or the use of a vacuum can achieve the former, however the exact requirements for the resist thickness are not easy to determine. Trade-offs exist between the required resolution and the ease of performing pattern transfer with the resist after exposure and development. The process latitude for the exposure can also be severely degraded if the resist becomes too thin.

17.4 Mask Requirements and Fabrication

In this Section we will describe the fabrication of a typical conformable mask suitable for near field exposure. Conformable amplitude masks have been fabricated on either 2 μm thick low stress silicon nitride Si_xN_y films grown on silicon substrates using low-pressure chemical vapour deposition (LPCVD), or on thicker (100–150 μm) glass or fused silica masks; fabrication of the silicon nitride masks will be presented in detail here. Membranes of silicon nitride were formed by wet etching of the backside of the silicon substrate in 50% by weight potassium hydroxide (KOH) solution. Typically, a membrane 5×5 mm^2 square is formed in the centre of a larger sample, leaving an outer silicon supporting ring. The membrane mask-making process is illustrated in Fig .17.3.

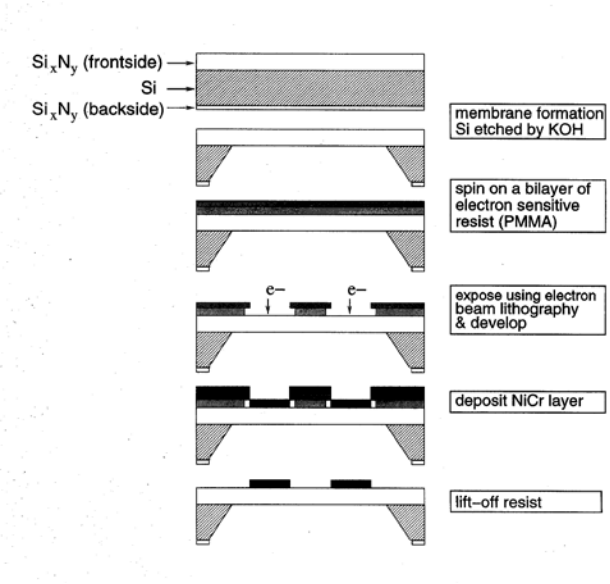

Fig. 17.3. Mask fabrication process, showing steps taken for forming the membrane and patterning the absorber features

Pattering of the mask patterns onto the Si_xN_y was performed using electron-beam lithography (EBL) onto membranes coated with a bilayer of polymethyl-methacrylate (PMMA). The bilayer resist was used to obtain an undercut profile desirable for the lift off metallisation process that was used to form the mask patterns. Arrays of 30 nm thick NiCr metal gratings of varying duty cycle were used to define the opaque regions on the mask. The linewidths in the gratings vary from 2 μm down to 60 nm. A typical amplitude mask with 130 nm gratings, isolated lines, and dense lines of NiCr patterns on a silicon nitride membrane is shown in Fig. 17.4.

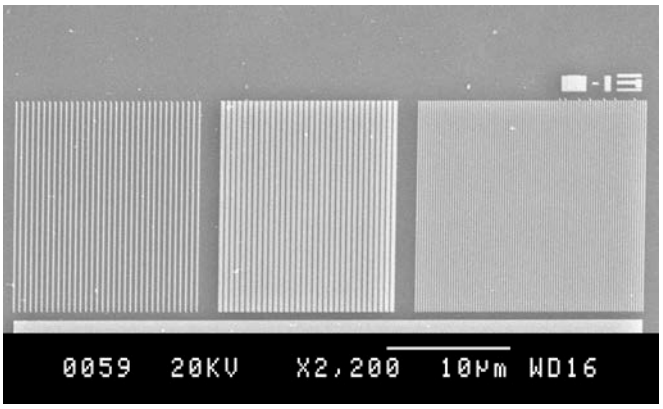

Fig. 17.4. Scanning electron microscope image of a typical membrane mask patterned with 25-nm thick NiCr gratings. The pattern on the left is isolated 130 nm lines on 390 nm period, the middle pattern contains 260 nm wide lines on 390 nm period, and the right-hand side pattern is a grating with 260 nm period (130 nm lines and spaces)

Other types of mask material, including glass or fused silica substrates have also been successfully employed, and these are generally more robust than the thin nitride membrane masks. However, obtaining conformal contact over large areas with these thicker masks in not so reliable. In addition, a subtractive process has been developed for forming the absorber patterns, using reactive-ion etching (RIE) of tungsten in a sulphur hexafluoride (SF_6) plasma; EBL in PMMA is used for pattern definition in this case also. This process reduces the occurrence of unwanted protrusions (so-called 'lift-off tags') that can sometimes prevent intimate contact in certain areas, leading to poor definition of sub-wavelength patterns.

17.5 Pattern Definition

ENFOL exposures were performed using a conventional mask aligner with mercury arc lamp having broadband illumination with wavelengths between 313 and 600 nm.

17.5.1 Exposure Conditions

A commercial *g*-line photoresist (Shipley S-1805) can be used, but has to be thinned to provide sub-wavelength thickness when spun onto a silicon substrate. A vacuum chuck ensures that the substrate and membrane mask are in intimate contact. Optimum results for reproducing 50 nm features were obtained using photoresist diluted 1:4 in PGMEA (60 nm thickness after spin coating) and an exposure time of 70 s. It should be noted that no strong feature-size dependent exposure times have been observed in these experiments. This has been demonstrated by the ability to pattern micron-scale and nanometre-scale features at the same time and from the same mask

17.5.2 Resist Requirements

Photoresist thickness is a major factor that determines the resolution limits and quality of patterns defined by ENFOL. The optimum resist thickness of 60 nm is required to ensure that the exposure is performed in the evanescent near field of the mask. For thinner resist layers, pattern transfer using RIE becomes difficult and for thicker resist layers the resolution degrades due to diffraction. Fig. 17.5(a) shows a partially resolved pattern exposed for 70 s into a 125 nm thick resist layer. The equivalent exposure into a 60 nm resist layer is shown in Fig. 17.5(b). Similar resolution degradation is observed if the mask and substrate are not held in conformable contact. These results illustrate the need to have significant exposure from the evanescent field close to the aperture plane of the mask in order to attain sub-wavelength features.

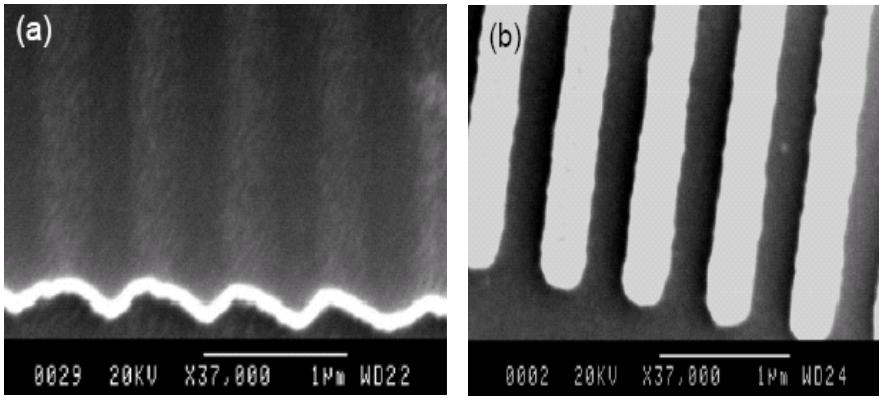

Fig. 17.5.(a) Partially resolved pattern formed by ENFOL exposure into 125 nm thick resist. (b) Pattern clearly resolved, obtained by exposing resist with the optimum thickness of 60 nm. Subtractive pattern transfer has been used to transfer the pattern in (a) and (b) into the silicon substrate to a depth of 100 nm

17.5.3 Overcoming the Diffraction Limit

Scanning electron microscope (SEM) images of high-resolution ENFOL-defined patterns are shown in Fig. 17.6. The patterns have been dry etched approximately 100 nm deep into silicon to facilitate imaging. Fig. 17.6(a) shows a 280 nm period grating formed by exposure through a mask with 70 nm isolated lines. After exposure, development and dry etching, the line width has been reduced to less than 50 nm, and there is some line edge roughness (LER) evident. It should be noted that the width of these lines is less than $\lambda_{min}/7$, where λ_{min} is the minimum exposing wavelength (365 nm). The period is approximately 0.77 λ_{min}.

Fig. 17.6(b) shows a 280 nm period grating formed by exposure through a mask with 70 nm apertures, the negative of the mask pattern used for Fig. 17.6(a). These 70 nm apertures are less than $\lambda_{min}/5$ wide, however, the exposure time for this pattern is the same as for patterns with large features. This indicates that there is no significant attenuation of the incident light through these sub-wavelength apertures. High transmission through sub wavelength sized circular aperture arrays has been previously reported (Ebbesen et al. 1998), and was attributed to plasmon resonances. In the ENFOL case, we have rectangular aperture that are long with respect to the wavelength, and high transmission of one polarisation will always be possible.

Fig. 17.6(c) shows a 140 nm period grating formed in resist after exposure and development. This was exposed though a mask with 70 nm lines and 70 nm apertures. The lines in this pattern are discontinuous in places due to LER, however continuous lines are obtained for all patterns with periods greater than 200 nm. The grating period for the pattern shown in Fig. 17.6(c) is well below the diffraction limit for an equivalent projection lithography system. For normal incidence coherent illumination at wavelength λ the minimum resolvable period p_{min} in a projection optical lithography system is (Rai-Choudhury 1997)

$$p_{\min} = \frac{\lambda}{NA} \tag{17.1}$$

where NA is the numerical aperture of the system . The maximum ***possible*** NA is equal to the refractive index of the imaging medium, n, which is 1.6 for the photoresist we are using.

Therefore, the best result that projection lithography into this photoresist could achieve would be p_{min} = 228 nm for the shortest available exposure wavelength in our source (λ = 365 nm). The structure shown in Fig. 17.6(c) has a period 40% smaller than this diffraction limit. Index-matched projection lenses are not generally used so in practice a projection optical lithography system is limited to $NA < 1$. If, together with this, we consider the peak exposing wavelength transmitted through the masks (λ = 436 nm) then p_{min} = 436 nm and the structure shown in Fig. 17.6(c) has a period which is approximately 1/3 of the diffraction limit for the equivalent projection system.

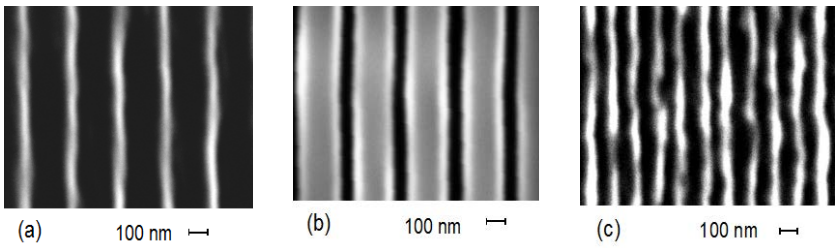

Fig. 17.6. Scanning electron microscope images of patterns produced using ENFOL and subsequent reactive ion etching: (a) 280 nm period grating exposed through a mask with 70 nm lines, (b) 280 nm period grating exposed through a mask with 70 nm apertures, and (c) 140 nm period grating exposed through a mask with 70 nm lines and 70 nm apertures

ENFOL's ability to pattern nanometre-scale and micron-scale features at the same time using the same exposure conditions is illustrated in Fig. 17.7. This figure shows a SEM micrograph for a grating structure of 2 μm wide lines with 1 μm spaces exposed and processed simultaneously with gratings that have periods down to 140 nm. These patterns show no pinhole defects and are uniform over the 40×40 μm^2 area of each grating on the substrate, and are uniform between fields distributed over the 5×5 mm^2 patterned area.

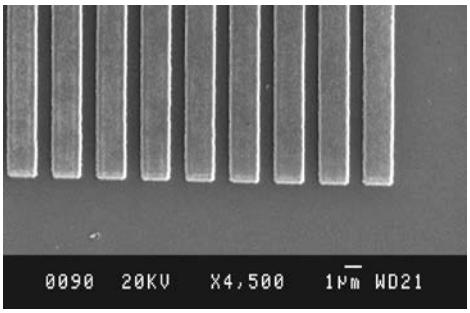

Fig. 17.7. Scanning electron microscope image of large feature patterns with 2 μm lines and 1 μm spaces produced using ENFOL. Patterns with feature sizes down to 70 nm have also been exposed and produced simultaneously from the same mask

17.6. Pattern Transfer

Transferring the photoresist patterns onto the substrate is an essential step in device fabrication. The challenge with ENFOL is performing pattern transfer using the ultra-thin resist layers that are necessary to achieve sub-diffraction limited resolution. Both subtractive (etching) and additive (lift off) pattern transfer techniques compatible with the ultra-thin resists, will be described in this section.

17.6.1 Subtractive Pattern Transfer

Reactive ion etching (RIE) has been used for subtractive pattern transfer into silicon substrates, where the resist acts as an etch mask. Etching is particularly challenging with ultra-thin photoresist, since the gases used to etch the silicon also etch the resist. Using cryogenic temperatures suppresses the resist etching and a successful dry etching process has been developed as detailed in Fig. 17.8. A short SF_6 plasma etch was carried out at 173 K to transfer the resist pattern 120 nm deep into the silicon substrate. An anisotropic etch profile was achieved with an etch rate of 10 nm/s under the following conditions: SF_6 gas flow rate of 100 sccm, power density of 0.45 W/cm^2, etch pressure of 55 mTorr, and dc bias of –153 V.

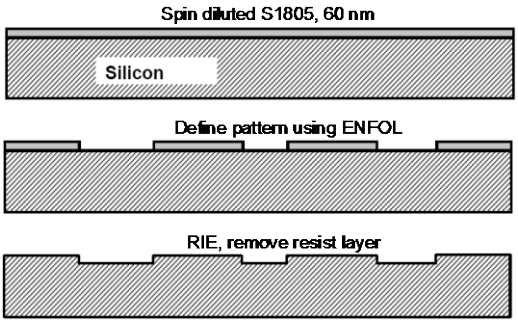

Fig. 17.8. Schematic diagram illustrating processing steps for subtractive pattern transfer using RIE. The pattern is defined first with the 60 nm thin resist and subjected to SF_6 plasma etching at 173 K

17.6.2 Additive Pattern Transfer

Additive pattern transfer involves the addition of metal films through a resist mask onto a substrate; the photoresist layer is then removed or lifted–off. Successful additive pattern transfer is not possible with ultra-thin resist. To achieve lift-off the resist should have a slightly undercut profile, and the resist thickness should be significantly greater than the metal being deposited. A trilayer scheme has been developed which improves the resist profile for lift off processes. The trilayer scheme consists of a top imaging layer (the ultra-thin photoresist), a barrier layer that acts as a hard etch mask (SiO_x) and an anti-reflection coating (ARC) bottom layer. Fig. 17.9 illustrates the trilayer additive pattern transfer technique that has been developed for ENFOL.

In this process a 130 nm thick film of a commercial ARC (XLT, Brewer Science) is first spun on the silicon substrates. This is then baked on a hot plate for 20 sec at 95°C followed by a one-minute bake at 170 °C. Following this a silicon oxide SiO_x barrier layer is thermally evaporated to a thickness of 16 nm, and the final ultra-thin photoresist imaging layer is then spun to give a uniform thickness of

45 nm. The sample is now ready for ENFOL exposure and development. Fig. 17.10(a) shows an atomic force microscope (AFM) image of a 270-nm period grating exposed into the imaging photoresist layer of a trilayer sample. As before, a clear sub-diffraction-limited pattern is evident, although there is a significant degree of LER. This AFM image of the photoresist prior to any pattern transfer process indicates that the LER is related to the resist not to any subsequent RIE.

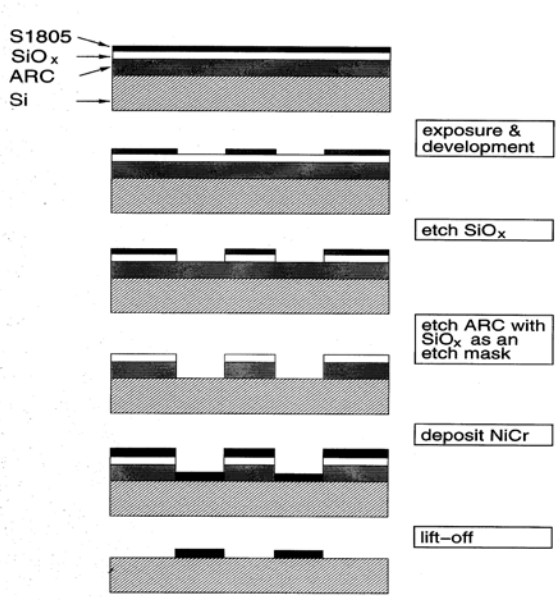

Fig. 17.9. Schematic diagram of the lift-off process used with trilayer additive pattern transfer scheme. The anti-reflection coating layer is 130 nm thick, SiO_x layer is 16 nm thick and the NiCr is 30 nm thick

After exposure and development of this imaging layer, the substrate is subjected to two RIE steps, to dry etch the SiO_x and the ARC respectively. The RIE recipes are given in Table 17.1. Fig. 17.10(b) shows a cross-sectional view of a 270 nm period grating after these RIE steps have been performed, and the transfer of the pattern into the full trilayer thickness is evident. The resist now has sufficient surface relief depth to allow lift-off of relatively thick films, however the required undercut sidewall profile of the etched trenches cannot be resolved with the AFM. This can only be determined from the success of the resultant lift-off. Any number of different materials could be deposited in the lift-off stage, and for this work a 30 nm NiCr film was then deposited by thermal evaporation and lifted off in MF320 developer. Fig. 17.10(c) shows an AFM image of the final 270 nm period NiCr gratings obtained with this trilayer pattern transfer technique. No degradation in pattern quality has resulted from the pattern transfer and lift-off processes, so this should be capable of being used for finer-period structures if the LER issues in the ENFOL exposure can be resolved.

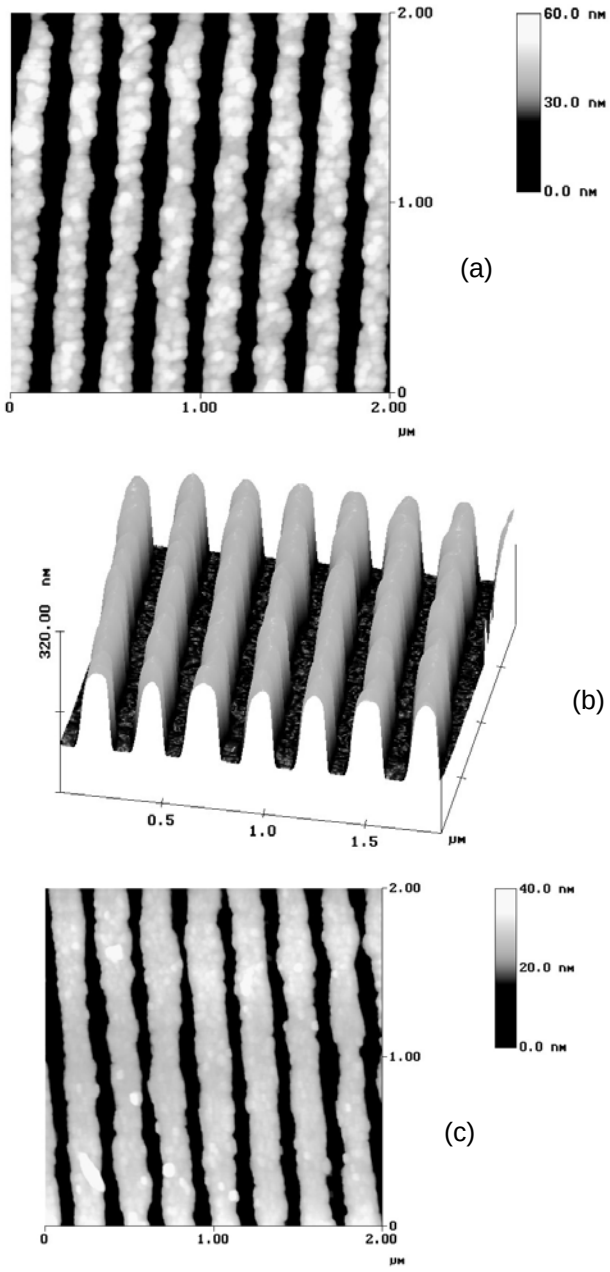

Fig. 17.10. AFM images of a 270 nm period grating: (a) in photoresist following exposure and development (note it is only 45 nm thick), (b) in ARC and SiO_x illustrating the improved profile following dry etching, (c) in 30 nm of NiCr following lift-off

Table 17.1. RIE recipes for SiO_x and ARC pattern transfer processes.

Gas	Etch rate (nm/min)	Pressure (mT)	Flow rate (sccm)	Power density (W/cm^2)	DC self bias (V)	Temp (°C)
CHF_3	20	3	15	0.45	506	22
O_2	90	6	20	0.45	489	22

17.7 Simulations

The resolution achievements of scanning near field optical microscopy of better than $\lambda/40$ (Betzig 1991) suggest the potential for equivalent resolutions in near field lithography. An understanding of the near field mechanisms responsible for evanescent exposure are required to guide future ENFOL studies and to explore its potential as a nanolithography technique. Simulations have been undertaken to study the near field region behind conducting gratings.

17.7.1 Simulation Methods and Models

The two-dimensional multiple multipole program (MMP) (Hafner 1990) has been used to investigate diffraction in the evanescent near field of metallic gratings, suspended in various dielectric media. MMP is a semi-analytic technique, in that the electromagnetic fields are approximated by a set of basis functions that are solutions to Maxwell's equations. The program numerically sets the coefficients to these basis functions to minimise the errors for the boundary conditions at matching points distributed along the boundary. Once the coefficients have been determined a full vector solution can be found at any point. Finite-difference time domain (FDTD) techniques have also been used to study ENFOL and related techniques, and these are in agreement with the MMP results. Simulations are performed for chrome transmission gratings of pitch p and thickness t suspended in a medium with index of refraction n. Fig. 17.11 illustrates a typical geometry that has been simulated and defines the Cartesian coordinate system and illumination polarisation. In general only the TM polarisation is considered as for gratings of this scale very little light TE light is transmitted due to the polarising nature of the grating (McNab and Blaikie 2000). A unit cell consisting of one period of the grating is computed while specialised periodic boundaries take into account the effects of surrounding conductors to obtain a solution for effectively an infinitely long grating. Note that, an evanescent exposure is defined here as an exposure where all the transmitted diffracted orders are evanescent. The zeroth propagating order is also generally present but does not provide contrast for photolithography as it does not contain any modulation in the x direction; it simply appears as an intensity offset. For incident illumination normal to the grating an evanescent exposure occurs when $p < \lambda/n$, where λ/n is the effective wavelength.

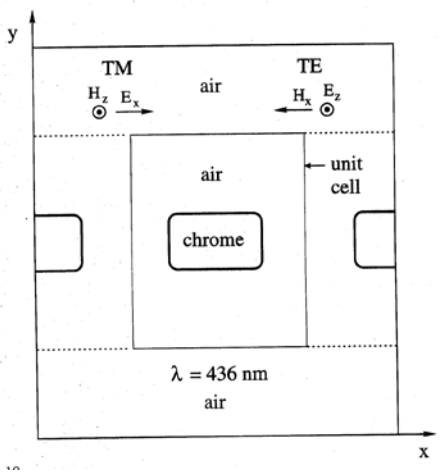

Fig. 17.11. Simulation model illustrating suspended chrome gratings mask to simulate exposure into a substrate held in intimate contact with the mask. The TE and TM polarisation orientations are indicated

17.7.2 Intensity Distribution

Fig. 17.12 shows the 2D normalised intensity $|E|^2/|E_{in}|^2$, where E_{in} is the incident electric field, for an evanescent exposure of a 140 nm pitch grating with Cr conductors (ε = -13.24 + *i*14.62), 40nm thick suspended in free space (n = 1).

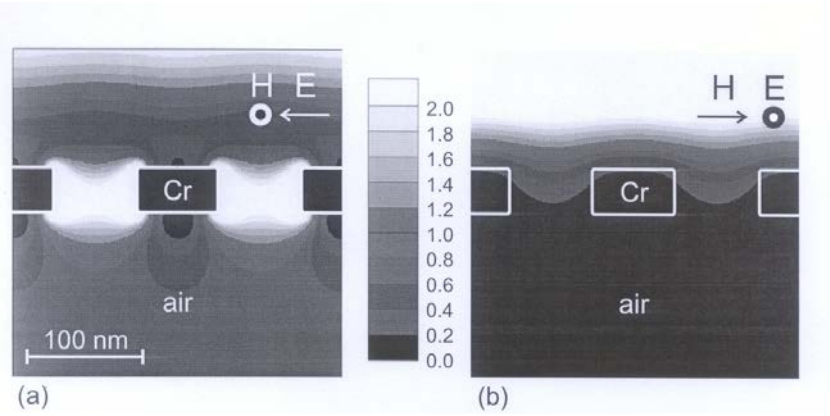

Fig.17.12. Normalised intensity distribution for a 140 nm pitch, 40 nm thick Cr grating in free space. The grating is illuminated from above by 436 nm TM polarized light (electric field E and magnetic field H directions are indicated). Contour plots of the normalised electric field intensity are shown $|E|^2/|E_{in}|^2$, where E_{in} is the incident electric field. The scale varies linearly from 0 (black) to 2.0 (white) in 10 linear steps

The grating is illuminated at normal incidence by TM polarised light with a wavelength λ = 436 nm. Line-plots of the intensity are presented in Fig. 17.13 for the same exposure conditions as in Fig. 17.13 extracted at the exit aperture of the grating, and then 10, 20 and 50 nm below the grating. These figures illustrate two of the characteristics of an ENFOL exposure – the decaying amplitude of the intensity as we move further below the grating, and strong edge enhancements that are evident close to the exit aperture of the grating, such as can be seen in Fig. 17.12(a).

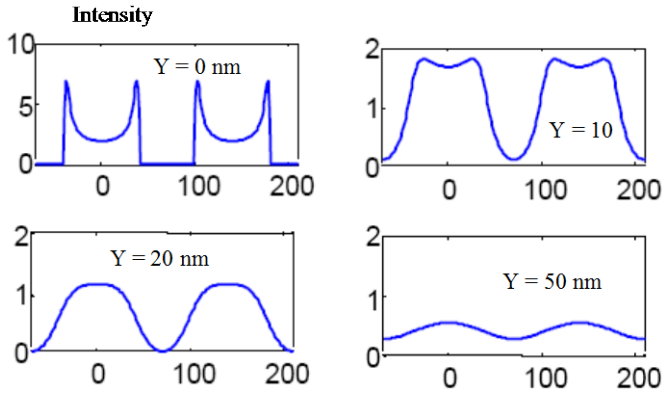

Fig. 17.13. Normalised intensity line plots for the simulation in Fig. 17.11. The line plots are taken at y = 0 (the exit plane of the grating), then at 10 nm, 20 nm, and 50 nm below the exit plane of the grating mask respectively

17.7.3 Depth of Field (DOF)

The depth of field (DOF) is a critical parameter for a lithography technique that relies on evanescent field components to expose photoresist. It defines the depth at which "sufficient" contrast is available for an exposure; but this is not a fixed value, it varies with different resist chemistries and different exposure conditions. We define the contrast *k* in the image at a distance *y* below the mask to be

$$k(y) = \frac{I_{\max}(y) - I_{\min}(y)}{I_{\max}(y) + I_{\min}(y)} \tag{17.2}$$

where I_{max} and I_{min} are the maximum and minimum intensities in the *x*-z plane a distance *y* below the mask. We will define the depth of field, DOF_k, as the depth below the grating at which the contrast *k* falls below a specified value.

Simulations of a conducting Cr grating suspended in free space have been performed and Fig. 17.14 plots DOF_k versus the grating pitch for various *k* factors.

These results show a linear relationship between grating pitch and depth of field, which is due to the near field nature of the exposure. In addition, the depth of field is greater for smaller *k* factors, as might be expected. This implies that the use of high contrast resists (which allow imaging at low *k* factors) will ease the ultra-thin-resist constraint imposed by the ENFOL technique. However, even for a contrast factor as low as $k = 0.3$, resist thicknesses below 100 nm are required to achieve resolution below 300 nm. The simulations also show that high contrast images are present in the near field regions of gratings with pitches as small as 20 nm, although in these cases the depth of field is less than 10 nm. This indicates the prospect for resolution of 20 nm pitch gratings in 3 nm of resist for $k = 0.5$. We believe that such resolution is experimentally achievable using new generation resist chemistries such as surface layer imaging resists (Herndon et al 1999) or self-assembled monolayer resists (Friebel et al 2000).

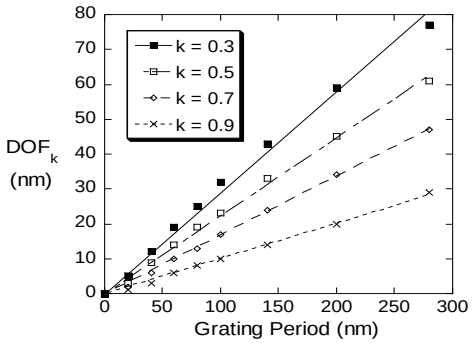

Fig. 17.14. Depth of Field (DOF_k) versus pitch p for simulated gratings plotted for k values of 0.3, 0.5, 0.7, and 0.9

The linear nature of the relationship between DOF_k and grating pitch can be qualitatively understood for an evanescent exposure by considering y^I_m, the depth at which each diffracted component decays to 1/e of its initial intensity (Loewen and Popov 1997),

$$y^I_m = \frac{1}{4\pi\sqrt{\frac{m^2}{p^2} - \frac{n^2}{\lambda^2}}} \tag{17.3}$$

where *m* is the diffracted order. From Eq. 17.3 it is evident that the higher the diffracted order, the faster its intensity decays. This has an impact on the exposure at the depth defined by DOF_k. For high values of *k* there exists a significant contribution from higher order ($m > 1$) evanescent components while at low *k* values there is generally only a significant contribution from the ±1 orders providing contrast. For gratings with deep sub-wavelength pitches $p << \lambda/n$, the $m = \pm 1$

components will dominate, and the linear relation $y^I_m \approx p/4\pi$ results from Eq. 17 3. Note that this is independent of λ and n, so we expect the resolution of ENFOL to be independent of these parameters for deep sub-wavelength gratings. This opens the prospect of choosing an exposure wavelength for optimal resist performance, by-passing the usually difficult task of designing resist performance for an optimal exposure wavelength. The choice of resist thickness is crucial for a successful exposure, firstly to obtain sufficient contrast and secondly to ensure adequate process latitude. It is clear from Fig. 17.14 that the resist thickness should be chosen according to the smallest feature pitch to be patterned. To improve process latitude, operation at a high k is preferable which requires reducing the resist thickness further for a given resist system.

Operating at low k values also increases the likelihood of exposure variation. As we move further away from the grating where the higher order evanescent components have disappeared, the intensity is dominated by the zeroth diffracted order, with transmission coefficient $T_0 = |E_0|^2/|E_{in}|^2$ where E_0 is the zeroth order electric field component. This is modulated by the contribution from the evanescent ±1 diffracted orders as shown in Fig. 17.12(d) for example. The exposure conditions are then heavily dependent on the magnitude of the T_0 component, which can fluctuates with factors such as changes in the duty cycle of the grating mask (% of conductor width to the grating pitch), as well as being sensitive to grating resonances. Variations in T_0 would make it difficult to expose gratings of different duty cycles in a single exposure. These effects are quantified in Fig. 17.15 for a 140 nm period grating suspended in air, in which $DOF_{0.5}$ and the maximum intensity at this depth are plotted. Increasing the duty cycle improves the DOF at the expense of exposure intensity. The improvement with larger duty cycles is due to the decreasing magnitude of the zeroth diffracted order relative to the other diffracted orders, which provide the contrast for the exposure. However, while an improvement in contrast is obtained, a longer exposure is required to compensate for a reduction in the intensity.

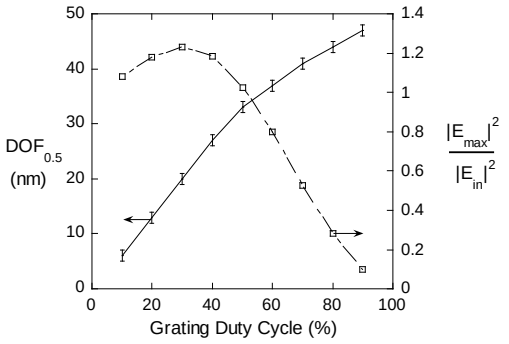

Fig. 17.15. Depth of Field $DOF_{0.5}$ for a 140 nm pitch grating (left axis) and the maximum intensity at this depth (right axis) versus duty cycle. The grating is suspended in free space and illuminated by 436 nm wavelength TM polarised light

17.7.4 Exposure Variations due to Edge Enhancements

Close to the exit aperture of the grating, high intensity enhancements occur at the grating conductor edges, as can be seen in Fig. 17.13(a) for example. These enhancements are due to the sharp discontinuity at the conductor corners, which encourages charge concentration in a manner analogous to a static electromagnetic problem. The static analogy becomes more reasonable as the grating period becomes much smaller than the wavelength. These enhancements are only evident with TM illumination as it is in the TM case that the sharp discontinuity in the *x*-component of electric field exists. The surface charge distributions that give rise to these field enhancements are known as surface plasmons – they give rise to electromagnetic fields with their maximum field at the surface and a characteristically exponential decay away from the surface (Raether 1998).

To investigate the effects of these edge enhancements simulations were carried out for a 140 nm pitch grating, in conditions identical to that of Fig. 17.11, except that the radius of curvature of the conductor corners was varied from 1 to 10 nm in steps of 1 nm. An increase in amplitude of the edge enhancements is evident as the radius is decreased, consistent with the static analogy. This is shown in Fig. 17.16, where we see the peak intensity at the exit aperture for a grating with a 1 nm radius is 25 times the incident intensity and 6 times greater than for a 10 nm radius. The relationship between the radius and peak intensity follows a power-law decay, as may be expected from a simple electrostatic analogy.

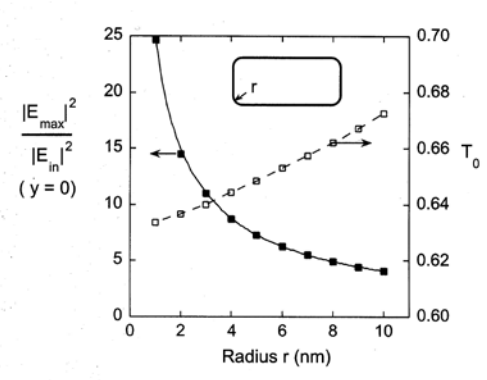

Fig. 17.16. Peak intensity at the grating exit aperture (left axis) and zeroth order intensity coefficient T_0 (right axis) versus the grating conductor radii of curvature r. The simulation model is the same as that in Fig. 17.11

The edge enhancements are relatively short-range. In 20 nm the peaks become less intense in amplitude than at the centre of the aperture, and their decay is independent of the radii of curvature. In the far field an increase in T_0 is evident at the expense of other diffracted orders as the radii are increased, as is shown in Fig. 17.16. This acts to reduce the contrast and, over the range of radii simulated, the zeroth transmitted order increases by 4%. This suggests that for reliable

lithography, maintaining as small a radius of curvature as possible on the mask edges is desirable. Line broadening also results from increasing the radii due to light leakage around the conductor corners and the creation of electric field components in the *x* direction over a broader region. Variability in the conductor profile during the production of the mask will therefore produce unpredictable duty cycles in the exposed resist.

ENFOL is also seen as a strong contender for printing onto curved surfaces due to the conformability of the mask. When printing onto curved surfaces, the light cannot be assumed to be collimated, and now a range of incident angles must be considered. Changes in the angle of incidence can result in placement biases in the lithography, but if the curvature of the substrate is known these can be accounted for in the design of the mask. The placement biases however will be susceptible to the conductor profile, particularly at angles varying greatly from normal incidence. Larger conductor radii can exaggerate the exposure broadening, making the mask profile more critical. To achieve acceptable tolerances for the lithography, the largest incident angle of light onto the surface to be printed needs to be determined which in turn specifies the control required on the conductor profile, for a particular photoresist thickness.

17.8 Nanolithography using Surface Plasmons

Surface plasmons have attracted renewed interest recently (www.surfaceplasmonoptics.org), particularly because they can give rise to some interesting electromagnetic phenomena. Ebbesen *et al.* demonstrated high transmission through an array of sub-wavelength apertures due to coupling between surface plasmons on either side of the metallic film. This transmission exceeded the Bethe limit for single apertures (Bethe 1944) by several orders of magnitude. A large amount of work has since been carried out, and sophisticated sub-wavelength structures have been devised to enhance the throughput from *single* sub-wavelength apertures and to provide a highly collimated far-field radiation pattern from such apertures.

In addition, surface plasmons have been identified as having a very important role to play in designing new materials that exhibit a *negative index of refraction* (Shelby 2001). It has been predicted that a lens made from such material will have resolution beyond the conventional diffraction limit – the so-called ‘Perfect Lens’ (Pendry 2000). Such a material requires both negative permeability and negative permittivity, however a near-field demonstration of perfect lensing should be possible in a material with only one of these negative, such as a metal illuminated close to its plasma frequency. Recent theoretical work also suggests that metal nanowire composites could be used to realise negative refraction at optical wavelengths.

Surface plasmons play an important role in ENFOL, and by manipulating their generation and propagation some interesting new near-field lithography modes can be developed and explored (Blaikie 2001; Luo 2004). Some of these are re-

viewed here, although it should be noted that this field is very much in its infancy at this point in time.

17.8.1 Evanescent Interferometric Lithography (EIL)

The principle of evanescent interferometric lithography (EIL) is based on the nature of interference between evanescent diffracted orders, particularly close to a resonance of the grating that is illuminated with UV light (Blaikie 2001).

Fig. 17.17 compares the intensity distribution for two identical TM-illuminated chrome gratings. Both have a period of 270 nm and are imbedded in a medium with a refractive index $n = 1.6$. For this grating period and refractive index the cutoff for first order diffraction is at a wavelength of 432 nm, and this is the illumination wavelength chosen for Fig.17.16(a). In this case the ±1 diffracted orders, which propagate at close to a grazing angle, interfere to form a period-halved intensity distribution beneath the mask. Zeroth order diffraction is suppressed (the so-called Wood's anomaly) which results in a high contrast in the interference pattern. This near field interference mimics that obtained in conventional interferometic lithography, and the period halving effect is useful for giving a 2× reduction of the grating.

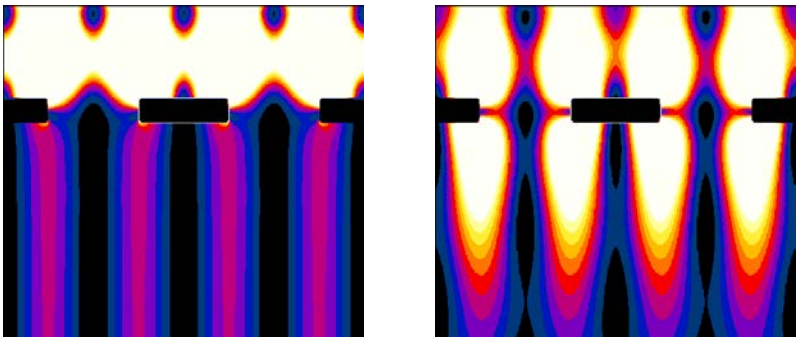

Fig. 17.17. Simulations of TM exposure through 280-nm period Cr gratings embedded in a dielectric material with refractive index n = 1.6. Exposure wavelengths are (a) 432 nm and (b) 438 nm

In Fig. 17.17(b) the illumination wavelength has been increased to 438 nm, for which the ±1 diffracted orders are now evanescent. No far field diffraction would be obtained for this grating, however a strong, high-contrast interference pattern is retained in the near field. The intensity and contrast in this interference pattern decay exponentially away from the mask; in this case the depth of field is more than 300 nm, which would be adequate for exposure of conventional resist layers. The most interesting point to note about the EIL exposure is the intensity enhancement that can be obtained. The peak near field intensity in Fig. 17.17(b) is

more than five times the incident intensity, which would result in a significant lowering of exposure time compared with conventional interferometric lithography.

17.8.2 Planar Lens Lithography (PLL)

Following Pendry's prediction that a planar silver layer excited near its plasma frequency could produce a sub-diffraction-limited resolution image in the near field simulations and experiments have been performed to test this for near field lithography (Blaikie 2002; Melville 2004). The system that has been studied is shown in Fig. 17.18. Within a free-space background medium a metal grating of period p and thickness t_1 is illuminated from above with transverse magnetic (TM) polarised light of wavelength λ. At a distance f_1 beneath the exit plane of the grating there is a planar layer (PL) of thickness t_2. In a simplistic negative refraction picture the presence of this layer is predicted to cause an image of the mask pattern to be formed a distance $f_2 \approx f_1$ below its bottom surface (see ray diagram). Silver (Ag) is chosen for the metallic material as its complex permittivity, $\varepsilon = \varepsilon' + j\varepsilon''$, has a negative real part and small complex part for blue/UV wavelengths used for photolithography. For example, at $\lambda = 341$ nm its complex permittivity is $\varepsilon = -1 + 0.4$, (Johnson and Christy 1972) which is closely index-matched to the surrounding free-space medium. This is the illumination wavelength chosen for this work – tuning the illumination wavelength so that the layer is index-matched to some other dielectric medium will produce similar results.

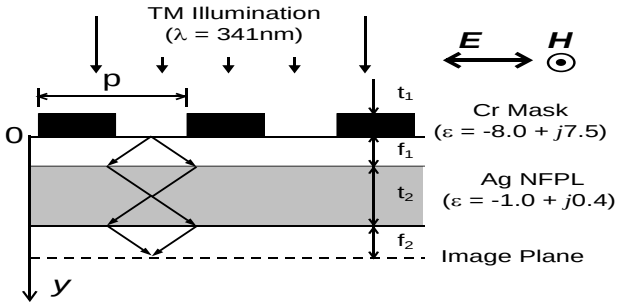

Fig. 17.18. Geometry & illumination condition for the near field planar lensing simulations

Simulation results comparing the near field intensity distribution with and without a silver NFPL are shown in Fig. 17.19. Exposures are for a mask with period $p = 140$ nm, which is sub-diffraction limited. Fig. 17.19(a) shows the case with $f_1 = 20$ nm and $t_2 = 40$ nm. Two sub-diffraction-limited images of the mask are observed, the first in the center of the PL, and the second at a distance of $f_2 = 23$ nm below it. This second image could be used for nanolithography by placing a photoresist in this plane. This second image is superimposed on a background intensity that decays with distance below the PL, making the image

difficult to discern. This arises because the mask period is sub-diffraction-limited, and the image is constructed from evanescent fields beneath the NFPL. Nonetheless, the peak intensity in the second image is 74% of the incident intensity, so exposure times for this new technique should be similar to those for conventional contact lithography with the same source and resist. The intensity distribution for the non-PL case shown in Fig. 17.19(b) shows no similar lensing effects. There is a region directly beneath the mask in which a shadow image forms, but the intensity and visibility of this image decays smoothly with distance. This simple near field intensity distribution has been used to obtain sub-diffraction-limited resolution, but there is a requirement of intimate mask-resist contact for higher resolution.

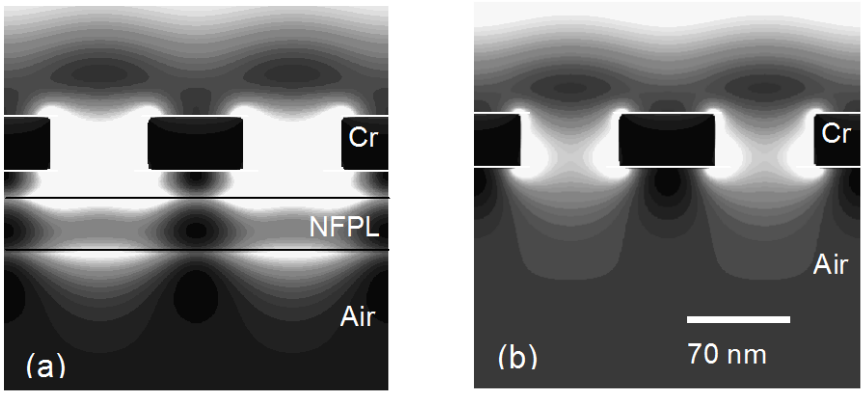

Fig. 17.19. Near field intensity profiles for a 140 nm period grating illuminated at 341 nm, (a) with a near field planar lens (NFPL) and (b) without a NFPL. The normalised intensity is plotted from 0 (black) to 2 (white) in linear steps of 0.1

Experimental verification of PLL has been achieved (Melville 2004), although not yet with sub-diffraction-limited resolution. Fig. 17.20 shows comparative AFM images of 1 μm-period gratings exposed with and without the PL layer. The exposure time was 120 s and the development time was 8 s in both cases. These AFM images clearly show that the silver PL is effective in forming a near field imaging of the the mask, whereas in the proximity exposure all resolution for the 1 μm-period grating is lost. Whilst there is some degree of overexposure for the proximity exposure of Fig. 17.20(a), faithful reproduction of the mask object is not achieved even for shorter exposures (Melville 2004). This is the first experimental demonstration of near field imaging through a silver layer, and efforts are now underway to determine the resolution of the technique. By reducing the thickness of the silver and spacers layers improved resolution can be obtained, and sub-wavelength resolution has been achieved by using a 50 nm thick silver layer,

as shown in Fig. 17.21. The fidelity of the micron-scale feature is much improved in this case, and resolution down to a period of 250 nm is evident.

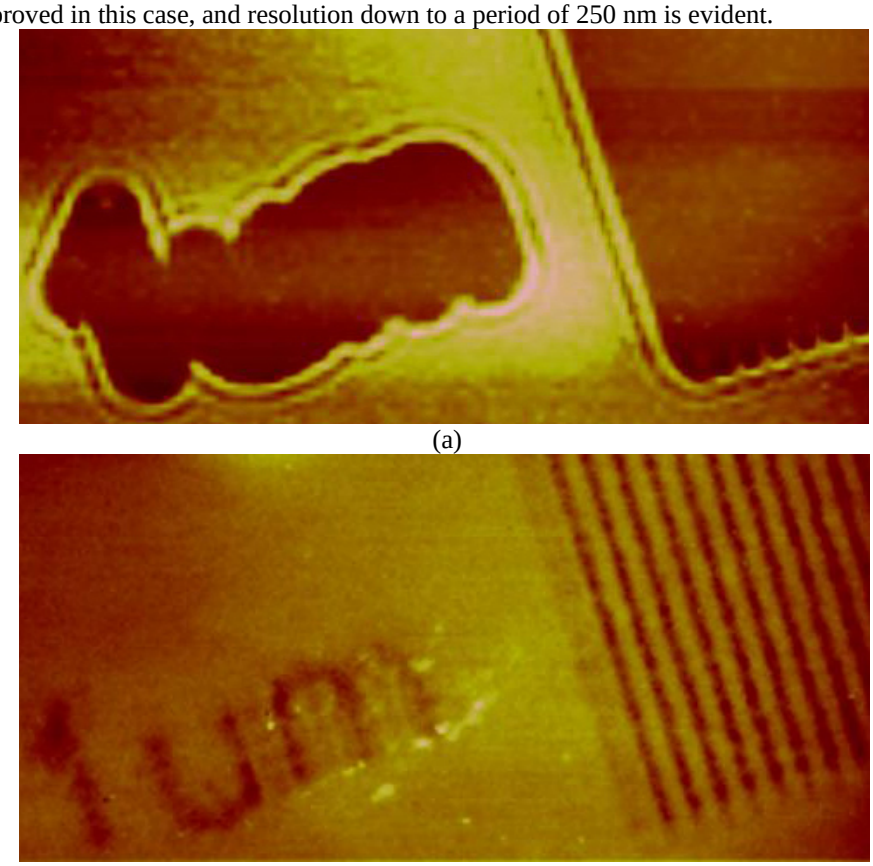

(a)

(b)

Fig. 17.20. Atomic force microscope (AFM) images of 1-micron period gratings exposed into 50 nm thick photoresist: (a) exposure performed with a 120 nm thick PMMA spacer; (b) exposure performed through a PMMA/silver/PMMA stack with 60nm/120nm/60nm thicknesses respectively

Simulations for the exposure geometries of Fig. 17.20 have been performed, and the results are shown in Fig. 17.22. In this case the FDTD method was used to perform these simulations. The simulation results for the proximity exposure are shown in Fig. 17.22(a), and it is clear that the pattern in the resist layer is of low contrast. There are some near field interference features apparent in this simulation, which may have been expected to give rise to discernable patterns in the developed resist. However the simulation is only for a single wavelength, and for the broadband source used for the exposure many such interference pattern will superimpose to produce a featureless final exposure pattern. For the PL exposure shown in Fig. 17.22(b) there is a much clearer image present in the resist layer, as observed in the experimental results. In this case the broadband nature

of the exposure does not change the simulation results significantly, as the self-filtering nature of the silver PL only allows significant transmission at this wavelength.

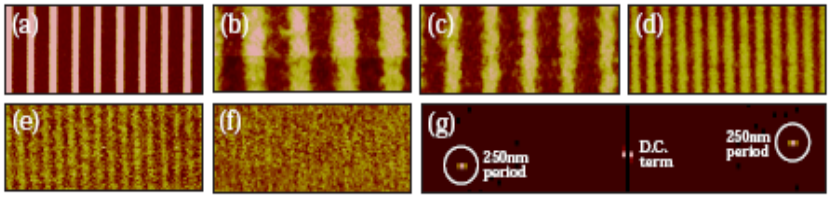

Fig. 17.21. AFM scans show resist profiles exposured through a 25 nm|50 nm|10 nm − PMMA|Ag|SiO_2 mask stack. Feature fidelity at (a) 1 µm, (b) 500 nm, (c) 420 nm, (d) 350 nm, (e) 290 nm, and (f) 250 nm periods are shown. Part (g) shows the two-dimensional Fourier transform of (f), confirming the presence of the 250 nm period features

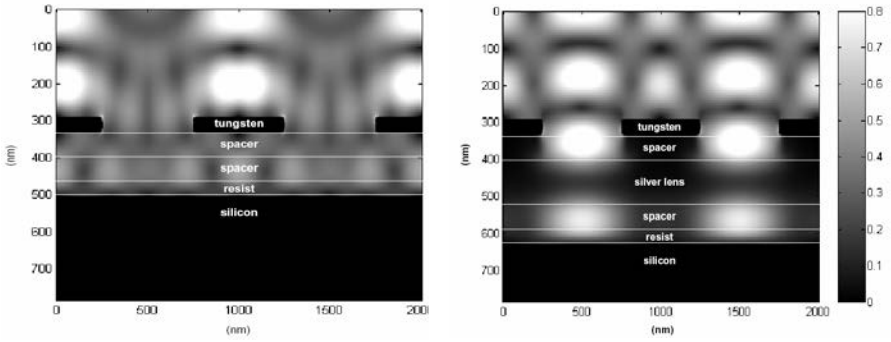

Fig. 17.22. Finite difference time domain (FDTD) simulations for the exposures shown in Fig. 17.20. The illumination wavelength is 341 nm in both cases and the spacer material is PMMA

17.8.3 Surface Plasmon Enhanced Contact Lithography (SPECL)

Another interesting effect was observed during the study of PLL. It was noted that the quality of the image *above* the planar lens could be enhanced by surface plasmons on the underlying metallic film, and this effect has been termed Surface Plasmon Enhanced Contact Lithography (SPECL). This is illustrated in Fig. 17.23, which compares the near field intensity profiles for two 140 nm period Cr gratings illuminated at 341 nm, embedded in a medium with refractive index of 1.6.

Fig. 17.23(a) shows the usual ENFOL case, where the material beneath the mask has a uniform refractive index (or is an index-matched stack). In this case the image has poor contrast at the exit plane of the mask, has a limited depth of

focus, and that at depths greater than 80 nm beneath the mask an image reversal occurs. These effects reduce the process latitude for faithful patterning in this case.

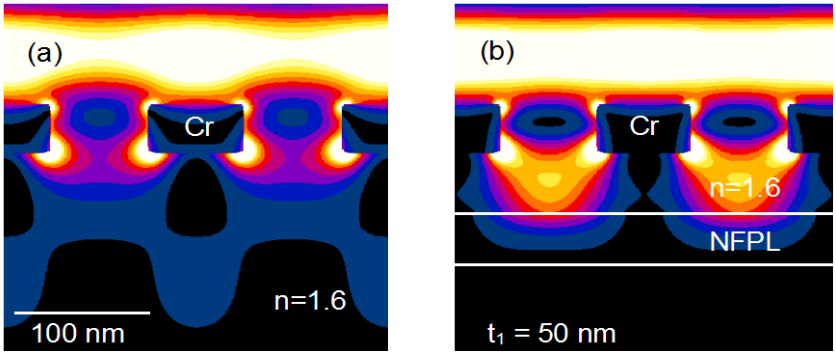

Fig. 17.23. Near field intensity profiles for a 140 nm pitch grating embedded in a medium with refractive index of 1.6 and illuminated at 341 nm: (a) with the entire underlying material index matched with n = 1.6; and (b) with a 40 nm thick silver layer 50nm beneath the mask to show the surface plasmon enhanced contact lithography (SPECL) effect. The normalised intensity is plotted from 0 (black) to 2 (white) in linear steps of 0.2

The addition of a SPECL layer within the resist stack can significantly improve the depth of field and process latitude, as is shown in Fig. 17.23(b). In this case a 40 nm thick silver layer is included 50 nm beneath the mask. The contrast at the exit plane of the mask is improved, and high contrast without image reversal is preserved throughout the entire resist layer. This improvement is attributed to the generation of surface plasmons on the underlying silver layer, which illuminate from beneath in addition to the incident illumination from above. This goes against conventional wisdom that dictates that the best resolution in a multilayer resist is obtained when all the layers are index matched.

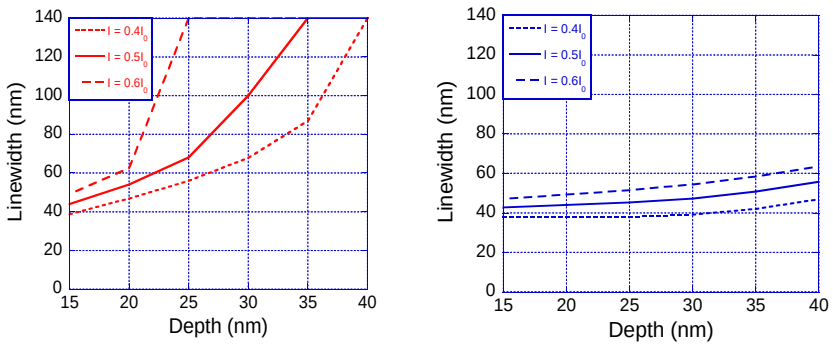

Fig. 17.24. Linewidth as a function of depth beneath the exit plane of the mask for the two intensity distributions shown in Fig. 17.23(a) index matched substrate; (b) a 40 nm thick

silver layer 50 nm beneath the mask. Linewidths are shown for the iso-intensity contours $I = 0.4I_0$ (dotted), $0.5I_0$ (solid) and $0.6I_0$ (dashed)

The improvement in process latitude is shown further in Fig. 17.24, which plots expected pattern linewidth versus depth for the two intensity distributions shown in Fig. 17.23. These are extracted from iso-intensity contours at $I = 0.4I_0$, $0.5I_0$ and $0.6I_0$, a ±20% variation about the middle value. In the case of the index-matched substrate (Fig. 17.24(a)) the linewidth for the $I = 0.5I_0$ exposure increases by more than a factor of three between depths of 15 nm and 35 nm beneath the mask. This compares to the SPECL situation in which the linewidth increase is less than 20%. Variations in exposure intensity will also be less critical for SPECL. A 20% increase in exposure intensity will increase the linewidth 30 nm beneath the mask by more than 40% for the index matched substrate exposure, whereas the equivalent increase for SPECL is less than 20%. This is encouraging for the development of a stable and repeatable process.

17.9 Conclusions

In the optical near field region the resolution limits for imaging are well below those for the far field. We have performed experimental and simulation studies of the implications of this for optical lithography, and in our ENFOL technique resolution below on fifth of the wavelength can routinely be achieved. Simulations indicate that there is scope to improve this resolution by at least another factor of two, which would allow sub-50 nm patterning without the need to use expensive deep-ultraviolet light sources; all of the experimental work presented here has been achieved with standard, low-cost mercury lamps.

The presence of surface plasmons on the metallo-dielectric interfaces in ENFOL-like exposures also opens a number of interesting possibilities. Firstly, the high electric fields associated with near-field plasmonic light confinement reverse the usual constrain of low intensity for near field imaging, showing that exposure times need not be sacrificed for resolution in the near field. Secondly, interference between evanescent orders can be used for interferometric lithography (EIL), resulting in exposed features smaller than the mask features; so near-field lithography is not solely limited to 1× reproduction. Thirdly, the tuned plasmonic properties of a silver film exposed near the i-line of mercury can be used to ‘project’ a near field image (PLL); so the constraint of hard contact can potentially be relaxed. Finally, plasmonic effects in an underlying layer of a resist stack can also be used to improve the depth of focus. These techniques are still in their infancy, and further work is needed to explore their true potential.

17.10 References

Chou SY, Krauss PR, Renstrom PJ (1995) Appl. Phys. Lett., 67, 3114.

Chou SY, Krauss PR, Zhang W, Gou L, Zhuang l (1997) J. Vac. Sci. Technol. B, 5, 2897
Khang DY, Lee HH (2000) Appl. Phys. Lett., 76, 870.
Bender M, Otto M, Hadam B, Vratzov B, Spangenberg B, Kurz H (2000) Microelectronic Engineering, 53, 233
Li M, Chen L, Chou S (2001) Appl. Phys. Lett. Vol 78, No 21, 3322
Austin MD, Ge H, Wu W, Li M, Yu Z, Wasserman D, Lyon SA, Chou SY (2004) Appl. Phys. Lett. ,84(26), 5299
Li M, Chen L, Zhang W, Chou SY (2003) Nanotechnology,14(1), 33
Rogers JA, Paul KE, Whitesides GM (1997) Appl. Phys. Lett., 71, 3773.
Lin BJ (3004) J. Microlithography Microfabrication and Microsystems, 3(3), 377
Owa S, Nagasaka H (2004) J. Microlithography Microfabrication and Microsystems,3(1) 97
Yamashita H, Amemiya I, Takeuchi K, Masaoka H, Takahashi K, Ikeda A, Kuroki Y, Yamabe M (2003) J. Vac. Sci.Technol. B 21 (6): 2645
Gallatin GM, Houle FA, Cobb JL (2003) J. Vac. Sci. Technol. B 21 (6): 3172
Smith HI, Efremow N, Kelly PL (1974) J. Electrochem. Soc. 121, 1503
Fischer UC, Zingsheim HP (1981) J. Vac. Sci. Technol. 19, 881
Davy S, Spajer M (1996) Appl. Phys. Lett. 69, 3306
Bouchiat V, Esteve D (1996) Appl. Phys. Lett. 69, 398
Blaikie RJ, Alkaisi MM, McNab SJ, Cumming DRS, Cheung R, Hasko DG (1999) Microelectronic Engineering, 46, 85.
Alkaisi MM, Blaikie RJ, McNab SJ, Cheung R, Cumming DRS (1999) Appl. Phys. Lett., 75, 5360.
Alkaisi MM, Blaikie RJ, McNab SJ (2000) Microelectronic Engineering, 53, 237
McNab SJ, Blaikie RJ, Alkaisi MM (2000) J. Vac. Sci. Technol. B 18, 2900
M.M. Alkaisi, R.J Blaikie, S.J. McNab, Adv. Mater, 13, No 12-13, 877, 2001.
McNab SJ, Blaikie RJ (2000) Appl. Opt. 39, 20
Smith HI (1969) Rev. Sci. Instrum. B 40, 729
Smith HI (1974) Proc. IEEE 62, 1361
White JC, Craighead HG, Howard RE, Jackel RE, Behringer LD, Epworth RW, Henderson DHI, Sweeney JE (1984) Appl. Phys. Lett. 44, 22
Smith HI, Efremow N, Kelly PL (1974) J. Electrochemical Soc. 121, 1503
Goodberlet JG (2000) Appl. Phys Lett. 76, 667
Goodberlet JG, Bryan LD (2000) Microelectronic Engineering 53, 95
Goodberlet JG, Kavak H (2002) Appl. Phys.Lett.81, 1315
Schmid H, Biebuyck H, Michel B, Martin OJF, Piller NB (1998) J. Vac. Sci. Technol B 16, 3422
Rogers JA, Paul KE, Jackman RJ, Whitesides GM (1997) Appl. Phys. Lett. 70, 2658
Paulus M, Schmid H, Michel B, Martin OJF (2001) Microelectronic Engineering, 57-8, 109-116
Levenson M (1993) Phys. Today 7, 28
Alkaisi MM, Blaikie RJ, McNab SJ (1998) J. Vac. Sci. Technol. B 16, 3929
Ono T, Esashi M (1998) Jpn. J. Appl. Phys. 37, 6745
HaefligerD A Stemmer, (2004) Ultramicroscopy 100(3-4):457-464
Luo XG, Ishihara T (2004) Japn. J. Appl. Phys. part1 (6B) 4017-40-21)
Ebbesen TW, Lezec HJ, Ghaemi HF, Thio T, Wolff PA (1998) Nature 391, 667
RaiChoudhury P (1997) (Ed.) Microlithography, Micromachining, and Microfabrication. Volume 1: Microlithography. SPIE Press, Washington, pp. 31-33
Betzig E, Trautman JK, Harris TD, Weiner JS, Kostelak RL (1991) Science, 251, 1468
Hafner C (1990) The Generalised Multiple Multipole Technique for Computational Electromagnetics, Artech, Boston, Mass. 1990.

Herndon MK, Collins RT, Holligsworth RE, Larson PR, Johnson MB (1999) Appl. Phys. Lett. , 4, 141.
Friebel S, Aizenberg J, Abad S, Wiltzius P (2000) Appl. Phys. Lett, 77, 2406.
Loewen E, Popov E (1997) Diffraction Gratings and Applications. Marcel Dekker
Raether H (1998) Surface Plasmons on Smooth and Rough Surfaces and on Gratings, vol.111, Springer Tracts in Modern Physics. Springer-Verlag
http://www.surfaceplasmonoptics.org
Bethe HA (1944) Phys. Rev. 66, 163
Thio T, Lezec HJ, Ebbesen TW, Pellerin KM, Lewen GD, Nahata A, Linke RA (2002) Nanotechnology 13, 429
Hibbins AP, Sambles JR, Lawrence CR (2002) Appl. Phys. Lett. 81, 4661
Baida FI, Labeke D (2003) Phys. Rev. B 67, 155314
Lezec HJ, Degiron A, Devaux E, Linke RA, Martin-Moreno L, Garcia-Vidal FJ, Ebbesen TW (2002) Science 297, 820
Martin-Moreno L, Garcia FJ, Lezec HJ, Degiron A, Ebbesen TW (2003) Phys. Rev. Lett. 90, 167401
Shelby RA, Smith DR, Schultz S (2001) Science 292, 77
Pendry JB (2000) Phys. Rev. Lett. 85, 3966
Blaikie, RJ, McNab SJ (2001) Appl. Opt. 40, 1692
Blaikie RJ, McNab SJ (2002) J Microelecron. Eng. 61 97
Melville DOC, Blaikie RJ, Wolf CR (2004) Appl. Phys. Lett. 84(22), 4403
Johnson PB, Christy RW (1972) Phys. Rev. B 6, 4370
Melville DOS, Blaikie RJ (2004) J. Vac. Sci. Technol. B 22 3470